SEASONAL RESPONSE OF ENERGY FOUNDATIONS DURING BUILDING OPERATION

By K.D. Murphy, M.S., S.M.ASCE[1] and John S. McCartney, Ph.D., P.E., M.ASCE[2]

Abstract: This paper focuses on the response of two full-scale energy foundations beneath an 8-story building during operation of a heat pump over a 658-day period. During circulation of fluid having temperatures ranging from 7 to 35 °C through the closed-loop heat exchangers within the foundations, the temperature of the reinforced concrete ranged from 9 to 30 °C and was relatively uniform with depth. Estimates of the average heat exchange per unit meter ranged from 91 to 95 W/m. The thermal axial strains during the first year of heating and cooling were elastic and recoverable, but a change in mobilized coefficient of thermal expansion occurred in the second year, potentially due to changes in interface shear stresses. The smallest magnitudes of thermal axial strains were observed at the top and bottom of the foundations due to the restraint provided by the overlying building and underlying bedrock. Issues were encountered in the interpretation of the thermal axial stresses, and were attributed to thermally induced dragdown and transient differences in temperature between the reinforced concrete and sensors. The maximum thermo-mechanical axial stress in the foundations was approximately 10 MPa, well within structural limits. The mobilized side shear stresses follow a nonlinear profile with depth, potentially due to the combined effects of thermal expansion and downdrag. The thermal axial displacements estimated at the foundation head relative to the toe ranged from -1.5 mm upward to 0.8 mm downward during heating and cooling of the foundation, respectively, which are not expected to affect the building.

[1] Engineer, Shannon and Wilson, Denver, CO, USA, kdm@shanwil.com.
[2] Associate Professor and Lyall Faculty Fellow, Department of Civil, Environmental and Architectural Engineering, University of Colorado Boulder, UCB 428, Boulder, CO 80309

INTRODUCTION

This paper presents data from a nearly 2-year long case study involving an assessment of the thermal and thermo-mechanical response of 2 energy foundations installed beneath an 8-story building in Denver, CO, USA. A preliminary evaluation of the response of these foundations was provided by McCartney and Murphy (2012), who reported data measured during construction and after the first 30 days of heat pump operation. This study provides novel contributions by presenting data collected over the course of two years of heat pump operation, including the temperatures of the heat exchange fluids measured using thermistors, as well as profiles of foundation temperatures and thermal axial strains measured using thermistors and vibrating wire strain gages embedded within the foundations at different depths. This data is suitable to assess the transient response of the energy foundations during daily and seasonal fluctuations in the temperature of the heat exchange fluid. Of particular interest are the changes in thermal axial strains, stresses, and displacements after seasonal cycles of heating and cooling.

BACKGROUND

The full-scale response of energy foundations has been assessed in several studies to evaluate their thermo-mechanical response in actual soil profiles under different conditions (Brandl 2006; Laloui et al. 2006; Bourne-Webb et al. 2009; Bouazza et al. 2011; Amatya et al. 2012; Olgun et al. 2012; McCartney and Murphy 2012; Murphy et al. 2014a; Murphy et al. 2014b). Although data from some of these tests were used to successfully validate soil-structure interaction design tools (Knellwolf et al. 2011) and thermo-elastic finite element models (Laloui et al. 2006; Ouyang et al. 2011; Wang et al. 2012), these studies did not focus on assessment of the long-term response of energy foundations after frequent reversals in temperature. Murphy et al. (2014a) characterized the thermo-mechanical performance of three energy foundations installed

in stiff sandstone beneath a 1-story building, and observed a linear thermo-elastic response during heating and subsequent cooling back to ambient temperature. However, they did not investigate the role of cooling the foundations below ambient conditions. Stewart and McCartney (2013) evaluated the transient response of a centrifuge-scale end-bearing type energy foundation installed within a layer of unsaturated silt during heating and cooling. They did not observe a significant change in thermal axial strain, stress, or displacement after four cycles of heating and cooling, even though thermally induced water flow was observed to change the stress state in the soil surrounding the foundation.

Many studies have evaluated the system thermal conductivity of full-scale energy foundations (Hamada et al. 2007; Gao et al. 2008; Lennon et al. 2009; Brettman and Amis 2011; Ozudogru et al. 2012; Loveridge and Powrie 2012; Murphy et al. 2014a; Murphy et al. 2014c). These studies have provided useful information on the thermal properties of energy foundations that can be used in design. Other studies on full-scale foundations included evaluations of the efficiency of thermal energy extraction (Brandl 2006; Ooka et al. 2007; Wood et al. 2009; Adam and Markiewicz 2009; Wood et al. 2010). Although these studies established that energy foundations can provide a sustainable source of thermal energy, only Brandl (2006) and Wood et al. (2010) showed an evaluation of the thermal performance of energy foundations under long-term heat pump operations.

ENERGY FOUNDATIONS CASE HISTORY

The 8-story building was supported by sixty drilled shaft foundations with a range of different dimensions and depths. This study is focused on two of the foundations that were converted to energy foundations and coupled to a conventional ground-source heat pump (GSHP) system which was already being incorporated into the building. The conventional GSHP system consists

of forty 101.6 mm-diameter boreholes, each extending to a depth of 143 m below grade, drilled in a parking lot outside of the building footprint. One of the foundations was installed under an interior column (Foundation A), and has a depth of 14.8 m and a diameter of 0.91 m. The other foundation is located under an exterior wall (Foundation B), and has a depth of 13.4 m and a diameter of 0.91 m. Both foundations serve as end-bearing elements in the Denver formation (claystone), and were designed to carry vertical loads of 3.84 and 3.65 MN, respectively. Each shaft contains a full-length reinforcing cage that is 0.76 m in diameter with nine #7 vertical reinforcing bars tied to #3 lateral reinforcing hoops spaced 0.36 m on center. A reinforced slab on grade with a thickness of 150 mm was cast at grade level. Foundation A includes three loops of polyethylene tubing with an inside diameter of 44 mm installed within the reinforcing cage, while Foundation B includes four loops. Each loop consists of a single length of tubing that was bent in the middle and fed through the bottom of the cage, with the inlet and outlet tubes on opposite sides of the reinforcing cage. At the bottom of the reinforcing cage, the loops were pulled to the side so that they would not cross the central axis of the foundation. Pictures of the reinforcing cages with the locations of the heat exchanger tubing are shown in McCartney and Murphy (2012). At the head of each foundation, the loops were connected in parallel using joints of different diameters so that all of the loops would have balanced flow of heat exchange fluid.

The site stratigraphy consists of urban fill atop a sandy gravel layer atop weathered claystone bedrock from the Denver formation (referred to as Denver Blue Shale). The thicknesses of the soil layers along with measurements from field tests are shown in Figure 1. The foundations were installed using a 10 m-long casing embedded into the claystone layer due to the presence of the urban fill and sandy gravel layers near the soil surface. Although the groundwater table was not noted within the depth of exploratory drillings, a perched water table at a depth of 7 m below

92 grade was noted in a borehole that was approximately 20 m away from the foundations. Water
93 flow was observed into the hole around the casing for Foundation A, likely due to the presence of
94 a local perched water table. No drilling mud was used during construction. Six concrete
95 embedment vibrating wire strain gages (Model 52640299 from Slope Indicator of Mukilteo,
96 WA) and thermistors were incorporated into each foundation at the depths shown in Figure 1.
97 The vibrating wire strain gages were oriented longitudinally parallel to the axis of the foundation
98 and were attached to the lateral reinforcing hoops. One of the vibrating wire strain gages at a
99 depth of 3.2 m in Foundation A was damaged during installation, but all of the other sensors
100 were functional over the duration of this project (including the thermistor at a depth of 3.2 m in
101 Foundation A). A Geokon, Inc datalogger (Model 8002-16 LC-2×16) was used to record data
102 hourly, using an excitation frequency range consistent with the specifications from the strain
103 gage manufacturer. The VWSGs were positioned at depths within the shaft so that the axial
104 strain distribution throughout the entire shaft length during mechanical loading and temperature
105 changes could be characterized. In addition to the instrumentation in the foundations, four pipe-
106 plug thermocouples were installed in the plumbing manifold in the mechanical room to record
107 inlet and outlet fluid temperatures for each of the two energy foundations. The thermistor body is
108 insulated to minimize the impact of room temperature fluctuations on the measurements of the
109 temperature of the heat exchanger fluid. Fluid temperature measurements were recorded every
110 five minutes using Lascar EL-USB-TC data loggers. The motivation for using the faster
111 sampling rate was to capture the temperatures during both short-term and long-term operations
112 of the heat pump. More details of the site, the conventional geothermal system, and the
113 foundation installation process are provided by McCartney and Murphy (2012).
114

RESULTS

Thermal Behavior

The heat exchange fluid used in the ground-source heat pump system is a mixture of 10% methanol and 90% water by volume. The temperatures of the heat exchange fluid entering and exiting Foundations A and B are shown in Figures 2(a) and 2(b), respectively. The outside air temperature for Denver, CO is shown in Figure 2(c) for comparison. Operation of the heat pump started on December 29th, 2011, so the data shown reflects nearly two full cycles of heating and cooling of the foundations. The temperatures of the heat exchange fluid entering the foundations, which range from 5 to 35 °C, depend on the operation of the eight heat pumps used to supply the heating and cooling demands of each floor. Because the heat pumps can independently access the fluid circulating through the system, it is possible for them to move heat from one floor to another as well as moving heat to or from the subsurface. Variable speed pumps are used to circulate fluid through the borehole field and the energy foundations, as well as through the tubing connecting each heat pump within the building. The flow through the two energy foundations was restricted by partial closure of ball-valves in the inlet header to minimize the chances for preferential flow through the foundations due to their shorter length than the conventional GSHP boreholes. The flow rate through the foundations may change depending on the pressure differential through the system (due to changes in fluid viscosity), which will affect the rate of heat transfer. Unfortunately, the fluid flow rate was not monitored continuously during operation of the GSHPs, so it is not possible to calculate the transient heat exchange per unit meter for each of the foundations.

The differences in the inlet and outlet fluid temperatures, $\Delta T_{in\text{-}out}$, also shown in Figures 2(a) and 2(b), can be used to assess the magnitude of heat exchange between the building and the

138 energy foundations. As the demand for thermal energy from the building changes, the heat
139 pumps will change the temperature of the fluid entering the foundations. During the winter and
140 summer months, the difference in fluid temperatures ranges between ±2 °C. This indicates that
141 relatively steady heat exchange between the ground and building occurs during the summer and
142 winter seasons. The occasional instances in the winter where the inlet fluid temperatures are
143 greater than the outlet temperatures may be due to the response of the heat pumps to the
144 occasional warm winter days reflected in the air temperature in Figure 2(c). Although the
145 difference in fluid temperatures during the spring and fall appears to show much more significant
146 fluctuations of ±10 °C, these results likely do not to reflect the heat exchange capabilities of the
147 energy foundations. The fluid flow through the foundations may be lower during the spring and
148 fall seasons when there is less demand from the foundations as the heat pumps are able to move
149 heat between the different floors of the building. Due to the uncertainty of the flow rate in the
150 spring and fall, the differences in fluid temperatures measured in the summer and winter of each
151 year best represent the heat exchange characteristics of the energy foundations.

152 Although the actual heat exchange fluid flow rates through each foundation were not
153 monitored, it is still possible to estimate the average heat exchange per unit meter for each of the
154 foundations using an estimate of the average flow rate. The circulation pump is capable of
155 supplying 1155 liters/min under a maximum pressure of 1550 kPa to overcome the head loss in
156 the length of tubing within the borehole field (11,440 m of vertical tubing plus additional headers
157 and couplings). As the length of tubing within the energy foundations is approximately 2% of
158 that in the borehole field, and flow through the energy foundations are restricted by the ball
159 valves, it is assumed that the average flow rate through the energy foundations is 2% of the
160 maximum flow rate from the pump, or 19.8 liters/min. This average flow rate is consistent with

recommendations for ground-source heat exchangers having similar length (Jeppesen 2010), and is sufficient to lead to turbulent flow conditions in the tubing (i.e., the Reynolds number of 8202 is sufficiently greater than the threshold value of 4000 to have turbulent flow). Based on this average flow rate, the average heat flux can be estimated as follows:

$$\dot{Q} = \Delta T \dot{V} \rho_{fluid} C_{fluid} \quad \textbf{(1)}$$

where ΔT is the difference between the supply and return fluid temperatures in K (T_{supply} and T_{return}, respectively), $\dot{V}$ is the average fluid flow rate (3.3×10^{-4} m^3/s), ρ_{fluid} is the mass density of the fluid (987.2 kg/m^3 at 25 °C), and C_{fluid} is the specific heat capacity of the fluid [4.0184 kJ/(kgK)]. Using these calculations, the averages of the absolute values of the heat transfer per unit length were 91 W/m for Foundation A and 95 W/m for Foundation B. Although it may not be appropriate to compare values of heat transfer per unit length for different energy foundations due to the effects of local site geology and groundwater effects, the average values estimated for these foundations are consistent with those reported by Bourne-Webb (2013) for foundations with similar length-diameter ratios (16.3 and 14.7 for Foundations A and B, respectively). The greater heat transfer in Foundation B compared to Foundation A may have been due to the extra loop in this foundation, although the gain in heat transfer for the extra length of heat exchanger does not appear to be significant.

The thermistors at different depths within each of the foundations were used to monitor temperatures within the reinforced concrete foundations on an hourly basis. Seasonal changes in the temperature profiles within the foundations before operation of the heat pump started were reported by McCartney and Murphy (2012). They observed a depth of seasonal fluctuations of approximately 5 m, with the near-surface foundation temperature ranging from 4 to 18 °C. An insulating effect of the building slab was observed in the near-surface foundation temperatures in

Foundation A compared to those in Foundation B. Time series of the temperature at different depths in the foundations after heat exchange operations started are shown in Figures 3(a) and 3(b) for Foundations A and B, respectively. The gap in the time series occurred because of a programming issue with the datalogger, which resulted in data not being recorded for 3 months. Nonetheless, the trends in the data are clear despite this gap. During heat exchange operations, the temperatures of the foundations were relatively uniform with depth, and ranged from 10 to 32 °C. Despite the insulating effect of the grade beam and building slab, slight differences in temperature were noted near the grade beam compared to the rest of the foundations. Further, the thermistor at the top of Foundation B showed slightly greater changes in temperature than the result of the foundation as the foundation is located under an exterior wall of the building, making it more sensitive to variations in ambient air temperature than Foundation A which is under the center of the building slab. The changes in the temperatures of the reinforced concrete are shown in Figure 3(c) and 3(d) for Foundations A and B, respectively, with the reference temperature being the ambient ground temperature at the beginning of the heat pump operation on December 29, 2011. These values ranged from -5 to 16 °C.

Thermo-Mechanical Strain Response

The thermal axial strains ε_T were calculated from the measured axial strain ε by first subtracting off the mechanical axial strains $\varepsilon_{mechanical}$ due to the self-weight of the building, which were reported by McCartney and Murphy (2012). The sign of the measured strain values ε was defined such that positive strains denote compression to be consistent with geotechnical sign conventions. The values of mechanical axial strain in the foundations were constant after construction of the building was complete in October 2011. It

206 is assumed that there is negligible drift in the mechanical strain measured by
207 the strain gages over time. Next, the zeroed strain values were corrected to
208 account for thermal effects on the gage. During heating of the gage, the
209 vibrating wire will expand, causing the VWSG to appear to go into
210 compression instead of correctly showing expansion. The equation used to
211 define the thermal axial strains is as follows:

$$\varepsilon_T = [(\varepsilon - \varepsilon_{mechanical}) + \alpha_s \Delta T] \quad (2)$$

212 where α_s is the coefficient of linear thermal expansion of the steel wire in the
213 gages (-12.0 $\mu\varepsilon$/°C), and ΔT is the change in temperature of the reinforced
214 concrete at the location of the gage. Use of this equation assumes that the
215 temperature of the steel wire is the same as that of the surrounding
216 reinforced concrete, which should be valid for seasonal temperature
217 fluctuations, but may not be valid for more rapid temperature fluctuations on
218 the order of several days due to the insulating effect of the air surrounding
219 the steel wire within the VWSG casing. The temperatures measured by the
220 thermistors likely best represents those of the gages but may be different
221 than the bulk reinforced concrete.

222 The thermal axial strains ε_T are shown in Figures 4(a) and 4(b) for
223 Foundations A and B, respectively. In these figures, positive strains indicate
224 compression while negative strains indicate expansion. The fluctuations in
225 thermal axial strain in both energy foundations correspond closely with the
226 timing of the fluctuations in temperature. Different from the foundation
227 temperatures, the thermal axial strain was observed to vary with depth in

the foundations, with the greatest expansion observed near the upper third of the foundations. Although the thermal axial strains appear to be relatively consistent within the foundation when comparing the trend from the first and second years of testing, the thermal axial strains near the bottoms of both foundations show a slight increasing trend with time. This is potentially due to ratcheting effects or thermo-plastic interface effects in the claystone layer.

The thermal axial strains behavior can be better evaluated by investigating the trends in the thermal axial strain plotted as a function of the change in temperature measured at the depth of each gage, shown in Figures 5(a) and 5(b) for Foundations A and B, respectively. The curves for all of the gages show some hysteresis, which indicates that there may be a ratcheting effect as the foundations are heated and cooled on a seasonal basis. The curves for the gages near the top of the foundations generally show the most linear response with the lowest amount of hysteresis. However, the curves for the gages near the bottom of both foundations show a change in slope during each seasonal fluctuation in temperature. Further, the hysteresis loops for these gages are not centered about the origin, with a downward shift after each heating and cooling cycle. It is possible that heating and cooling has a greater effect on the claystone than on the overlying cohesionless soils. Murphy et al. (2014a) observed a nearly linear response of the thermal axial strains versus temperature plots for energy foundations in dry sandstone, similar to those observed in this study for the

portions of the foundations in the cohesionless soils. Another explanation could be that the stresses within the claystone near the toe of the foundation may have been slowly redistributing from those present after installation, leading to greater restraint of the foundation and a smaller change in thermal axial strain for the same change in temperature.

A plot of the distribution in average mobilized coefficients of thermal expansion for each of the gages is plotted in Figure 5(c). This plot was created by taking the slopes of the thermal axial strain as a function of temperature change during the cooling cycle from summer 2012 until winter 2012. These mobilized coefficients of thermal expansion can be compared to that expected for unrestrained conditions $\alpha_{unrestrained}$. The thermal axial strain for unrestrained conditions can be calculated as follows:

$$\varepsilon_{T,unrestrained} = \alpha_{unrestrained}\Delta T \quad (3)$$

Unfortunately, the coefficient of thermal expansion for unrestrained conditions was not measured for the concrete mixture used at the site. Most studies have observed coefficients of thermal expansion for reinforced concrete unrestrained conditions ranging from -10 to -15 $\mu\varepsilon$/°C (Laloui et al. 2006; Murphy et al. 2014a; Goode et al. 2014). The trends in Figure 5(c) imply that the upper portions of the energy foundations have less restraint than the lower portions, as the mobilized coefficient of thermal expansion in these parts of the foundations are closer to the unrestrained value. The lower portions of the foundations are restrained by the bedrock at the toe and by potentially high side shear stresses in the claystone. The magnitudes of the

mobilized side shear stresses at the top of the foundations indicate that nearly free-expansion conditions occur, despite the stiffness provided by the grade beams of the 8-story building. Similar plots could be made for subsequent heating or cooling cycles. Although the shape of the distribution does not change significantly, the trends in Figures 5(a) and 5(b) show that the magnitude of the mobilized coefficients of thermal expansion will shift to the right, indicating a greater amount of restraint.

In order to define profiles of thermal axial strain representative of the energy foundation performance, instances in time when the energy foundations experienced different average changes in temperature were identified. These times were selected during the period when the foundation was cooling from a change in temperature of 14 to -5 °C during the period from summer to winter 2012. The temperature profiles for these average temperature increments are shown in Figures 6(a) and 6(b) for Foundations A and B, respectively. For these average changes in temperature, the temperature of the foundations were relatively uniform with depth.

Profiles of thermal axial strain corresponding to the average changes in temperature are shown in Figures 7(a) and 7(b) for Foundations A and B, respectively. The first observation is that the thermal axial strain profiles have relatively consistent shapes with depth during heating and cooling. The second observation is that as the energy foundations are cooled, the bottom portions of the foundations start to show contractile strains even though the change in temperature is still positive with respect to the original

296 temperature. It is possible that this phenomenon could be due to the fact
297 that the temperatures of the surrounding soil layers do not change as quickly
298 as the changes in temperature of the reinforced concrete. This would mean
299 that the soil could still be expanding while the foundation is contracting. It
300 could also be due to the effects of thermally induced volume changes of the
301 soil on the foundation superimposed on top of the expansion of the concrete.
302 Another observation is that the thermal axial strains are relatively high, an
303 issue that was noted by McCartney and Murphy (2012). For example, at the
304 extreme temperatures of 14 and -5 °C the thermal axial strains at all depths
305 in the energy foundations are completely in expansion and contraction,
306 respectively, but the mobilized coefficients of thermal expansion at some
307 depths are greater than -20 με/°C, which is much higher than that expected
308 for the unrestrained thermal expansion of reinforced concrete. It is possible
309 that the the large thermal axial strain values could be due to an issue in the
310 response of the VWSGs. However, the similarity in the trends and
311 magnitudes in thermal axial strain with depth in Foundations A and B
312 indicates that this would be a systematic issue with all of the gages. Instead,
313 this could be due to a mismatch between the temperature measured at the
314 location of the VWSG (representing the temperature of the gage and the
315 steel wire) and the temperature of the bulk reinforced concrete (which may
316 be closer to the temperature of the heat exchange fluid) when calculating
317 the mobilized coefficient of thermal expansion. The temperatures of the
318 outlet heat exchange fluid are up to 5°C different from those measured by

319 the thermistors. The fact that the average mobilized coefficients of thermal
320 expansion in Figure 5(c) are less than -13 με/°C indicates that the transient
321 differences in the temperature of the concrete and VWSG may be the reason
322 for the seemingly large expansions and contractions.

323 To investigate the behavior of the foundations at different extremes, the
324 thermal axial strain profiles at the end of the first and second extreme
325 heating events (to an average change in foundation temperature of 14 °C)
326 and the end of the first and second extreme cooling events (to an average
327 change in foundation temperature of -5 °C) can be compared. These profiles
328 are shown in Figures 8(a) and 8(b) for Foundations A and B, respectively. The
329 thermal axial strain profiles during the first extreme cooling event (February
330 2012) were relatively uniform with depth. The shapes of the thermal axial
331 strain profiles during the first extreme heating (August 2012) became more
332 nonlinear with depth, likely because the greater increase in temperature with
333 respect to the initial temperature caused more soil-structure interaction.
334 Greater expansion was observed in Foundation B than in Foundation A. After
335 the next cooling cycle (February 2013), the thermal axial strain profiles
336 retained a similar shape to that observed during the previous heating event,
337 albeit with greater magnitudes in the upper and lower parts of the
338 foundations. The impact of these greater magnitudes observed during the
339 second cooling cycle will be discussed in the next section. Although the
340 thermal axial strain profiles during the second extreme heating event
341 (August 2013) had a similar shape to that in the first extreme heating event

342 in both foundations, the magnitudes at the toe of Foundation A were
343 contractile during the second heating cycle. This could possibly have
344 occurred because the expansion during heating was not sufficient to
345 overcome the contractive thermal axial strains that may have become
346 locked into the bottom of the foundation during cooling.

347 *Thermo-Mechanical Stress Response*

348 The thermal axial stresses σ_T at different depths within the foundation can
349 be defined using the following equation:

$$\sigma_T = E(\varepsilon_T - \alpha_{unrestrained}\Delta T_{foundation}) \quad (4)$$

350 where E is the Young's modulus of reinforced concrete (30 GPa), ε_T is the
351 thermal axial strain at a given depth defined using Eq. (2), $\alpha_{unrestrained}$ is the
352 linear coefficient of thermal expansion of reinforced concrete, and $\Delta T_{foundation}$ is the change
353 in temperature of the foundation at the location of the strain measurement.
354 The product $\alpha_{unrestrained}\Delta T_{foundation}$ is the thermal axial strain for free expansion
355 conditions. Murphy et al. (2014a) were able to apply Equation (4) in a
356 straightforward manner to evaluate the thermal axial stresses during heating
357 of energy foundations in dry sandstone. However, they did not investigate
358 temperature reversals such as those encountered in this study. Because of
359 the issue mentioned in the previous section regarding the magnitude of the
360 thermal axial strains, it is difficult to select an appropriate value of $\alpha_{unrestrained}$
361 for the energy foundations in this study. However, this is expected to lead to
362 inaccurate results in the case that the energy foundations expand by a

363 greater amount. This was especially the case when the foundation was
364 cooled, when very large positive thermal axial strains were observed.

365 Another issue in using Equation (4) to evaluate the thermal axial stresses
366 from the calculated thermal axial strains is that ε_T and $\alpha_{unrestrained}\Delta T_{foundation}$
367 should have the same sign during heating or cooling. The value of
368 $\alpha_{unrestrained}\Delta T_{foundation}$ always has a sign that is the opposite that of the changes
369 in temperature shown in Figures 3(c) and 3(d), due to the negative sign of
370 $\alpha_{unrestrained}$. However, this product may be the opposite sign of the calculated
371 thermal axial strains at some instances in time during transient heating or
372 cooling. For example, this occurred when contractile thermal axial strains are
373 observed for positive changes in temperature in Figures 7(a) and 7(b). In
374 these instances in time, the thermal axial stress may be overestimated.

375 The issues mentioned above occurred even on the first cooling cycle,
376 which was a reason McCartney and Murphy (2012) used a global correction
377 factor to correct the thermal axial strain values from Equation (2), which
378 assumes a systematic issue with the measured strain values. This empirical
379 correction did not change the trends with height in the foundations, but
380 forced the thermal axial stresses to be in compression during heating and in
381 tension during cooling. Murphy (2013) also used a similar global correction
382 factor to define transient thermal axial stress profiles in the energy
383 foundations for the data presented in this paper. Although this approach may
384 be an equally valid assessment of the issues in the data, it is possible that
385 actual phenomena occurring in the energy foundations are causing the

386 issues in the evaluation of the thermal axial strain values, such as transient
387 differences in temperature in the foundation and VWSG and the effects of
388 thermally-induced dragdown forces superimposed atop the thermally
389 induced strains.

390 Due to the above issues, Equation (4) was not used in estimating the
391 transient changes in thermal axial stress from the thermal axial strains in
392 Figures 4(a) and 4(b). However, the thermal axial strains during extreme
393 heating to a change in temperature of 14 °C were not affected by the issues
394 mentioned above. A value of $\alpha_{unrestrained}$ of -13 με/°C was used in the analysis
395 based on the maximum value of the average mobilized coefficient of thermal
396 expansion in Figure 5(c). Accordingly, the thermal axial stresses generated
397 during extreme heating were added to the mechanical axial stresses due to
398 the building dead weight, as shown in Figures 9(a) and 9(b) for Foundations
399 A and B, respectively. Maximum thermo-mechanical axial stresses of 9.6-
400 10.1 MPa were observed near the bottom of Foundation A, while maximum
401 thermo-mechanical axial stress of 9.5-10.3 MPa were observed near the top
402 of Foundation B. The stresses at the two lowest depths in Foundation A
403 during the second extreme heating event were estimated by assuming a
404 thermal axial strain of zero in the calculation as the thermal axial strains
405 observed in Figure 9(b) were negative. Nonetheless, the observed
406 magnitudes are all much less than the compressive strength of concrete
407 (f'_c = 20 MPa), and the profiles of thermo-mechanical axial stress reflects
408 strong end bearing conditions with some head restraint (Amatya et al. 2012).

Although additional monitoring will permit evaluation of whether cyclic heating and cooling will lead to a greater increase in thermo-mechanical stresses over time, the only way that the thermal axial stresses would be greater than that shown in Figures 9(a) and 9(b) would be if the coefficient of thermal expansion for unrestrained conditions were greater than -13 με/°C.

Although it was not possible to accurately evaluate the tensile thermal axial stresses during cooling, it is likely from comparison of the magnitudes of the thermal axial strains during heating and cooling that the thermal axial stresses during cooling will not be sufficient enough to cause tensile stresses in the foundations. Accordingly, even though it was not possible to calculate these values, they are not relevant for the structural performance of these foundations. This may not be the case for semi-floating energy foundations that are lightly loaded, so extreme cooling should still be considered in the design of energy foundations.

Assessment of Mobilized Side Shear Stresses

The mobilized side shear stress $f_{s,mob}$ with depth during the first extreme heating event was calculated from the changes in thermal axial stress with depth, as follows:

$$f_{s,mob,j} = \frac{(\sigma_{T,j} - \sigma_{T,j-1})D}{4\Delta l} \quad \textbf{(5)}$$

where D is the shaft diameter and ΔL is the difference in height between thermal axial stress calculations for gages j and j-1. The mobilized side shear stress profiles are shown in Figure 10 for both foundations. A nonlinear profile with depth is observed in this figure due to the shapes of the thermal

axial stress profiles, which are influenced by the restraint provided by the overlying structure and the underlying claystone. As the foundation is completely in compression during the heating process and is expanding upward, the positive (upward) values of mobilized side shear stresses in the upper part of the foundation may reflect the combined effects of thermally induced dragdown and thermal expansion, a topic that deserves further study using advanced analyses. The mobilized side shear stresses are the greatest in the sandy gravel layer, with a downward direction and a magnitude ranging from 90 to 140 kPa. This magnitude of side shear resistance is consistent with that observed by Murphy et al. (2014a) for end-bearing energy foundations in stiff sandstone, but is greater than that measured by Stewart and McCartney (2013) for an end-bearing energy foundation in unsaturated silt.

Assessment of Thermo-Mechanical Displacement Profiles

The relative thermal axial displacements δ_T were estimated by integrating the thermal axial strain profiles with depth, as follows:

$$\delta_{T,i} = \delta_{T,i-1} + \frac{1}{2}\left(\varepsilon_{T,i-1} + \varepsilon_{T,i}\right)\Delta l \qquad \textbf{(6)}$$

where Δl is the distance between strain gages i and i-1. Profiles of relative thermal axial displacement are shown in Figures 11(a) and 11(b), assuming that the value of δ_T at the bottom of both foundations is zero. This is likely not true as the claystone is not perfectly rigid, so the displacement profiles are with respect to the potential movement of the toe. During transient cooling, a second null point is observed to move upward through the foundations. This may be due to a transitional effect caused by the soil pulling the foundation downward. The temperature

of the foundation is controlled by the heat exchange fluid, and the temperature effects on the surrounding soil will lag behind.

The top of Foundation A moves upward by -1.1 mm during heating and downward by 0.8 mm during cooling. Using a similar assumption, the top of Foundation B moves upward by -1.5 mm during heating and downward by 0.6 mm. In either case, the angular distortions defined using any column spacing in the vicinity of the foundations in the building are less than 1/5000. This magnitude of angular distortion is not sufficient to cause structural or architectural damage in the superstructure (Skempton and McDonald 1956).

CONCLUSIONS

The results from a thermo-mechanical evaluation of two full-scale energy foundations during heating and cooling operations of an 8-story building in Denver, Colorado confirm that the incorporation of ground-source heat exchange technology in drilled shaft construction can provide sustainable heat exchange with no major effects on the structural performance of the building. The conclusions that can be drawn from the data analysis include:

- The energy foundations exhibited steady heat exchange values in the summer and winter of each year. Estimates of the average values of heat exchange per unit meter of the energy foundations ranged from 91 to 95 W/m, which are consistent with observations from the characterization of other energy foundations reported in the literature.
- During circulation of fluid having temperatures ranging from 7 to 35 °C through the closed-loop heat exchangers within the foundations, the temperature of the reinforced concrete ranged from 9 to 30 °C and was relatively uniform with depth except near the surface. The average temperature changes in the foundations ranged from -5 to 14 °C.

- The thermal axial strain during the first year of heating and cooling were elastic and recoverable, but a change in mobilized coefficient of thermal expansion occurred in the second year, potentially due to changes in interface shear stresses.
- The shapes of the thermal axial strain in the second cycle of heating followed the same shape with depth as in the first cycle, indicating that the application of heating-cooling cycles led to a permanent effect on the thermal axial strain profiles. Issues were observed in the magnitude and trends of the thermal axial strains that were attributed to the effects of thermally induced dragdown and transient differences in temperature between the reinforced concrete and sensors, and deserve more evaluation using more advanced analyses.
- The greatest increase in the magnitudes of thermo-mechanical axial stresses in the foundations were observed near the toe of both foundations during heating. The greatest thermo-mechanical stress in Foundation A was observed near the base, and was approximately 10 MPa, while the greatest thermo-mechanical stress in Foundation B was observed at the head due to the shape of the mechanical stress profile, and also approximately 10 MPa. The thermal axial stress profiles during heating were consistent with the trends expected for an energy foundation with restraint provided by the overlying building and the underlying bedrock. It was not possible to evaluate the transient changes in thermal axial stresses due to the issues identified in the thermal axial strains without a more advanced analysis.
- The mobilized side shear stresses follow a nonlinear profile with depth potentially due to the combined effects of thermal expansion and thermally induced dragdown on the foundations.
- The thermal axial displacements estimated at the heat of the foundations ranged from -1.5 mm upward to 0.8 mm downward during heating and cooling, respectively.

- The values of thermal axial displacement and the thermo-mechanical axial stresses are within reasonable limits and are expected to cause to structural or architectural damage to the building.

Overall, the results presented in this paper indicate that energy foundation systems in complex soil layers may not always behave as a thermo-elastic system. In this case, a more complex heat transfer analysis would be needed to capture the effects of transient temperature changes within the foundation and in the surrounding soil, and a thermo-elasto-plastic model for the soil may be needed to capture the thermal effects on the soil-structure interaction response.

ACKNOWLEDGEMENTS

The authors acknowledge the support of Milender-White Construction Company, KL&A Structural Engineers, AMI Mechanical, Rocky Mountain Geothermal, and the Denver Housing Authority for agreeing to incorporate the energy foundations and instrumentation into the building. Financial support from National Science Foundation grant CMMI 0928159 is appreciated.

APPENDIX I. REFERENCES

Adam, D. and Markiewicz, R. (2009). "Energy from earth-coupled structures, foundations, tunnels and sewers." Géotechnique. 59(3), 229–236.

Amatya, B.L., Soga, K., Bourne-Webb, P.J., Amis, T. and Laloui, L. (2012). "Thermo-mechanical behaviour of energy piles." Géotechnique. 62(6), 503–519.

Bourne-Webb, P., Amatya, B., Soga, K., Amis, T., Davidson, C. and Payne, P. (2009). "Energy pile test at Lambeth College, London: Geotechnical and thermodynamic aspects of pile response to heat cycles." Géotechnique 59(3), 237–248.

Bouazza, A., Singh, R.M., Wang, B., Barry-Macaulay, D., Haberfield, C., Chapman, G., Baycan, S., and Carden, Y. (2011). "Harnessing on site renewable energy through pile foundations." Australian Geomechanics. 46(4), 79-90.

Bourne-Webb, P. (2013). "An overview of observed thermal and thermo-mechanical response of piled energy foundations." European Geothermal Congress. Pisa, Italy. 8 pg.

Brandl, H. (2006). "Energy foundations and other energy ground structures." Géotechnique. 56(2), 81-122.

Brettmann, T. and Amis, T. (2011). "Thermal conductivity evaluation of a pile group using geothermal energy piles." Proc. Geo-Frontiers 2011 (GSP 211). J. Han and D.E. Alzamora, eds. ASCE, Reston VA. pg. 499-508.

Gao, J., Zhang, X., Liu, J., Li, K. and Yang, J. (2008). "Numerical and experimental assessment of thermal performance of vertical energy piles: an application." Applied Energy. 85(10), 901-910.

533 Goode, J.C., III and McCartney, J.S. (2014). “Centrifuge modeling of energy foundations in
534 sand.” Physical Modeling in Geotechnics. Proc. 8th International Conference on Physical
535 Modelling in Geotechnics. Perth, Australia. January 14-17, 2014. Gaudin and White
536 (eds.). Taylor and Francis. London. pg. 729-736.
537 Hamada, Y., Saitoh, H., Nakamura, M., Kubota, H. & Ochifuji, K. (2007). “Field performance of
538 an energy pile system for space heating.” Energy and Buildings. 39(5), 517–524.
539 Hughes, P.J. (2008). Geothermal (Ground-Source) Heat Pumps: Market Status, Barriers to
540 Adoption, and Actions to Overcome Barriers. Oak Ridge Nat. Lab. Report ORNL-
541 2008/232.
542 Jeppesen, K.C. (2010). Fundamentals of Commercial Geothermal Wellfield Design. GHP
543 Systems, Inc. Brookings, SD. 32 pg.
544 Knellwolf, C. Peron, H., and Laloui, L. (2011). “Geotechnical analysis of heat exchanger piles.”
545 ASCE Journal of Geotechnical and Geoenvironmental Engineering. 137(10). 890-902.
546 Laloui, L., Nuth, M., and Vulliet, L. (2006). “Experimental and numerical investigations of the
547 behaviour of a heat exchanger pile.” International Journal of Numerical and Analytical
548 Methods in Geomechanics. 30, 763–781.
549 Lennon, D.J., Watt, E., and Suckling, T.P. (2009). “Energy piles in Scotland.” Proceedings of the
550 5th International Conference on Deep Foundations on Bored and Auger Piles, Frankfurt
551 (Van Impe, W.F. and Van Impe, P.O. (eds)). Taylor and Francis, London, UK.
552 Loveridge, F. and Powrie, W. (2012). “Pile heat exchangers: Thermal behaviour and
553 interactions.” Proc. ICE – Geotechnical Engineering. 166(GE2), 178-196.
554 McCartney, J.S. and Murphy, K.D. (2012). “Strain distributions in full-scale energy
555 foundations.” DFI Journal. 6(2), 28-36.

McCartney, J.S. and Rosenberg, J.E. (2011). “Impact of heat exchange on the axial capacity of thermo-active foundations.” Proc. Geo-Frontiers 2011 (GSP 211). J. Han and D.E. Alzamora, eds. ASCE, Reston VA. pg. 488-498.

Murphy, K.D. (2013). Evaluation of Thermal and Thermo-mechanical Behavior of Full-scale Energy Foundations. MS Thesis. University of Colorado Boulder. 136 pg.

Murphy, K.D., McCartney, J.S., Henry, K.H. (2014a). “Thermo-mechanical response tests on energy foundations with different heat exchanger configurations.” Acta Geotechnica. DOI: 10.1007/s11440-013-0298-4.

Murphy, K.D., McCartney, J.S., and Henry, K.H. (2014b). “Thermo-mechanical characterization of full-scale energy foundations.” From Soil Behavior Fundamentals to Innovations in Geotechnical Engineering: Honoring Roy E. Olson. GSP 233. M. Iskander, J.E. Garlanger, M. Hussein, eds. pg. 617-628. doi: 10.1061/9780784413265.050.

Murphy, K.D., Henry, K., and McCartney, J.S. (2014c). “Impact of horizontal run-out length on the thermal response of full-scale energy foundations.” Proc. GeoCongress 2014 (GSP 234), M. Abu-Farsakh and L. Hoyos, eds., ASCE, Reston, VA. pg. 2715-2714.

Olgun, G.C., Martin, J.R., Abdelaziz, S.L., Iovino, P.L., Catalbas, F., Elks, C., Fox, C., Gouvin, P. (2012). “Field testing of energy piles at Virginia Tech.” Proc. 37th Annual Conference on Deep Foundations, Houston, TX, USA.

Ooka, R., Sekine, K., Mutsumi, Y., Yoshiro, S. SuckHo, H. (2007). “Development of a ground source heat pump system with ground heat exchanger utilizing the cast-in place concrete pile foundations of a building.” EcoStock 2007. 8 pp.

577 Ouyang, Y., Soga, K. and Leung, Y.F. (2011). "Numerical back-analysis of energy pile test at
578 Lambeth College, London." Proc. Geo-Frontiers 2011 (GSP 211). J. Han and D.E.
579 Alzamora, eds. ASCE, Reston VA. pg. 440-449.
580 Ozudogru, T., Brettmann, T., Olgun, G., Martin, J., and Senol, A. (2012). "Thermal conductivity
581 testing of energy piles: Field testing and numerical modeling." ASCE GeoCongress 2012.
582 Oakland, CA. March 25-29th, 2012. pg. 4436-4445.
583 Wang, W., Regueiro, R., Stewart, M.A., and McCartney, J.S. (2012). "Coupled Thermo-Poro-
584 Mechanical Finite Element Analysis of a Heated Single Pile Centrifuge Experiment in
585 Saturated Silt." Proc. GeoCongress 2012 (GSP 225), R.D. Hryciw, A. Athanasopoulos-
586 Zekkos, and N. Yesiller, eds., ASCE, Reston, VA. pg. 4406-4415.
587 Skempton, A.W. and MacDonald, D.H. (1956), "Allowable settlement of buildings." Proc.
588 Institute of Civil Engineers. London, Part 3, Vol. 5, pp. 727- 768.
589 Stewart, M.A. and McCartney, J.S. (2013). "Centrifuge modeling of energy foundations under
590 cyclic heating and cooling." ASCE Journal of Geotechnical and Geoenvironmental
591 Engineering. 11 pg. DOI: 10.1061/(ASCE)GT.1943-5606.0001061.
592 Wood, C.J., Liu, H. and Riffat, S.B. (2009). "Use of energy piles in a residential building, and
593 effects on ground temperature and heat pump efficiency." Géotechnique. 59(3), 287–290.
594 Wood, C.J., Liu, H., and Riffat, S.B. (2010). "An investigation of the heat pump performance
595 and ground temperature of a piled foundation heat exchanger system for a residential
596 building." Energy. 35, 4932-4940.

LIST OF FIGURE CAPTIONS

Fig. 1. Schematics of the scale model energy foundation including locations of instrumentation

Fig. 2. (a) Inlet and outlet fluid temperatures in Foundation A, (b) Inlet and outlet fluid temperatures in Foundation B; (c) Minimum and maximum surface air temperatures

FIG. 3. Foundation temperatures: (a) Temperature fluctuations in Foundation A; (b) Temperature fluctuations in Foundation B; (c) Change in temperature in Foundation A; (d) Change of temperature in Foundation B

FIG. 4. Thermal axial strains: (a) Foundation A; (b) Foundation B

FIG. 5. Thermal expansion evaluation: (a) Thermal axial strain with change in temperature for Foundation A; (b) Thermal axial strain with change in temperature for Foundation B; (c) Distribution in average mobilized coefficients of thermal expansion of the two energy foundations

FIG. 6. Profiles of temperature for different average changes in foundation temperature: (a) Foundation A; (b) Foundation B

FIG. 7. Thermal axial strain profiles: (a) Foundation A: (b) Foundation B

FIG. 8. Thermal axial strains after cycles of extreme temperature changes: (a) Foundation A; (b) Foundation B

FIG. 9. Thermo-mechanical (TM) axial stresses during extreme heating to an average change in temperature of 14 °C: (a) Foundation A; (b) Foundation B

FIG. 10. Mobilized side shear resistance profiles during extreme heating to an average change in temperature of 14 °C for Foundations A and B

FIG. 11. Thermal axial displacements: (a) Foundation A; (b) Foundation B

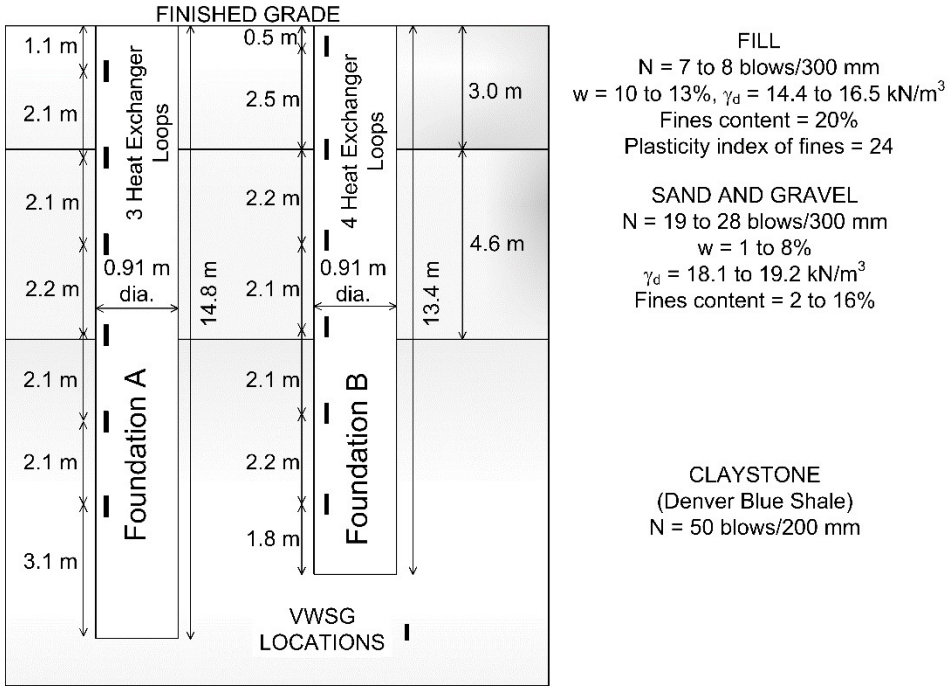

624

625 **Fig. 1**. Schematics of the scale model energy foundation including locations of instrumentation

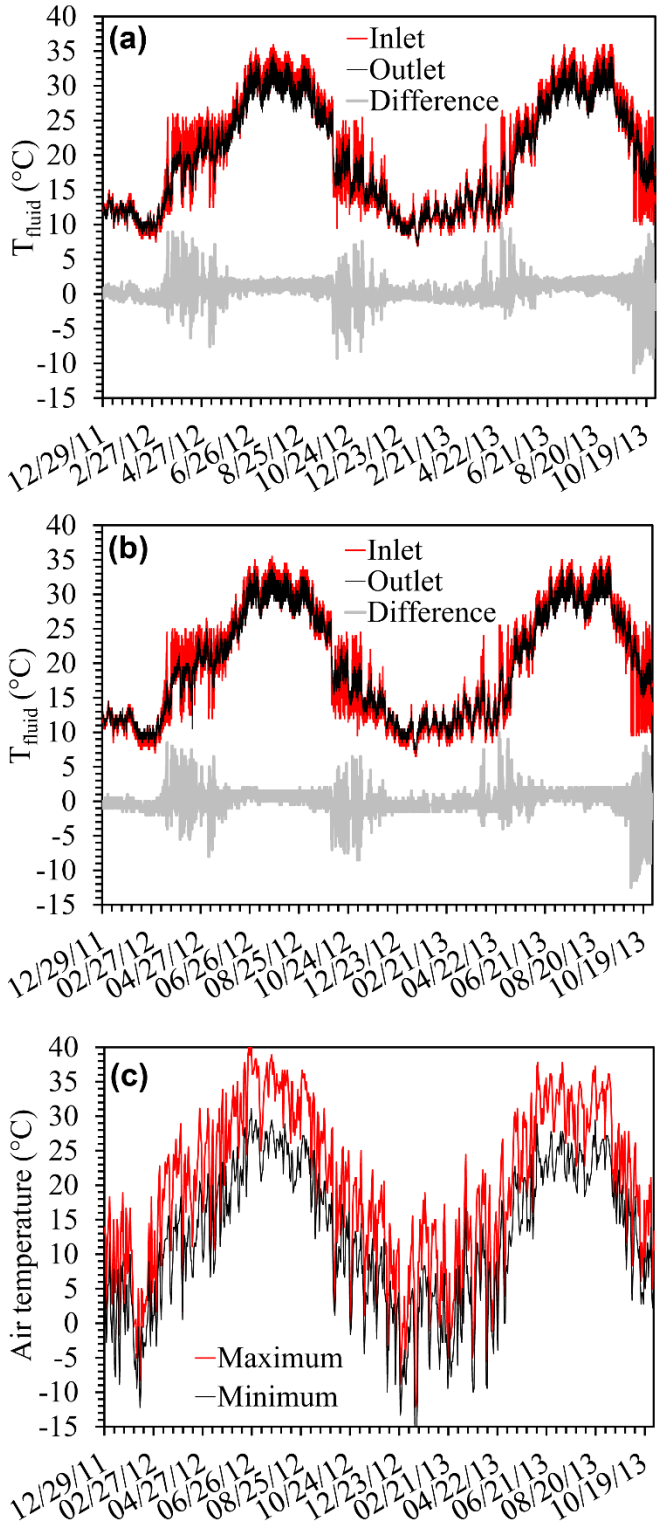
(a)
Inlet
Outlet
Difference
T_{fluid} (°C)
40
35
30
25
20
15
10
5
0
-5
-10
-15
12/29/11
2/27/12
4/27/12
6/26/12
8/25/12
10/24/12
12/23/12
2/21/13
4/22/13
6/21/13
8/20/13
10/19/13
(b)
Inlet
Outlet
Difference
T_{fluid} (°C)
12/29/11
02/27/12
04/27/12
06/26/12
08/25/12
10/24/12
12/23/12
02/21/13
04/22/13
06/21/13
08/20/13
10/19/13
(c)
Air temperature (°C)
Maximum
Minimum
12/29/11
02/27/12
04/27/12
06/26/12
08/25/12
10/24/12
12/23/12
02/21/13
04/22/13
06/21/13
08/20/13
10/19/13

626

627 **Fig. 2**. (a) Inlet and outlet fluid temperatures in Foundation A, (b) Inlet and
628 outlet fluid temperatures in Foundation B; (c) Minimum and maximum
629 surface air temperatures

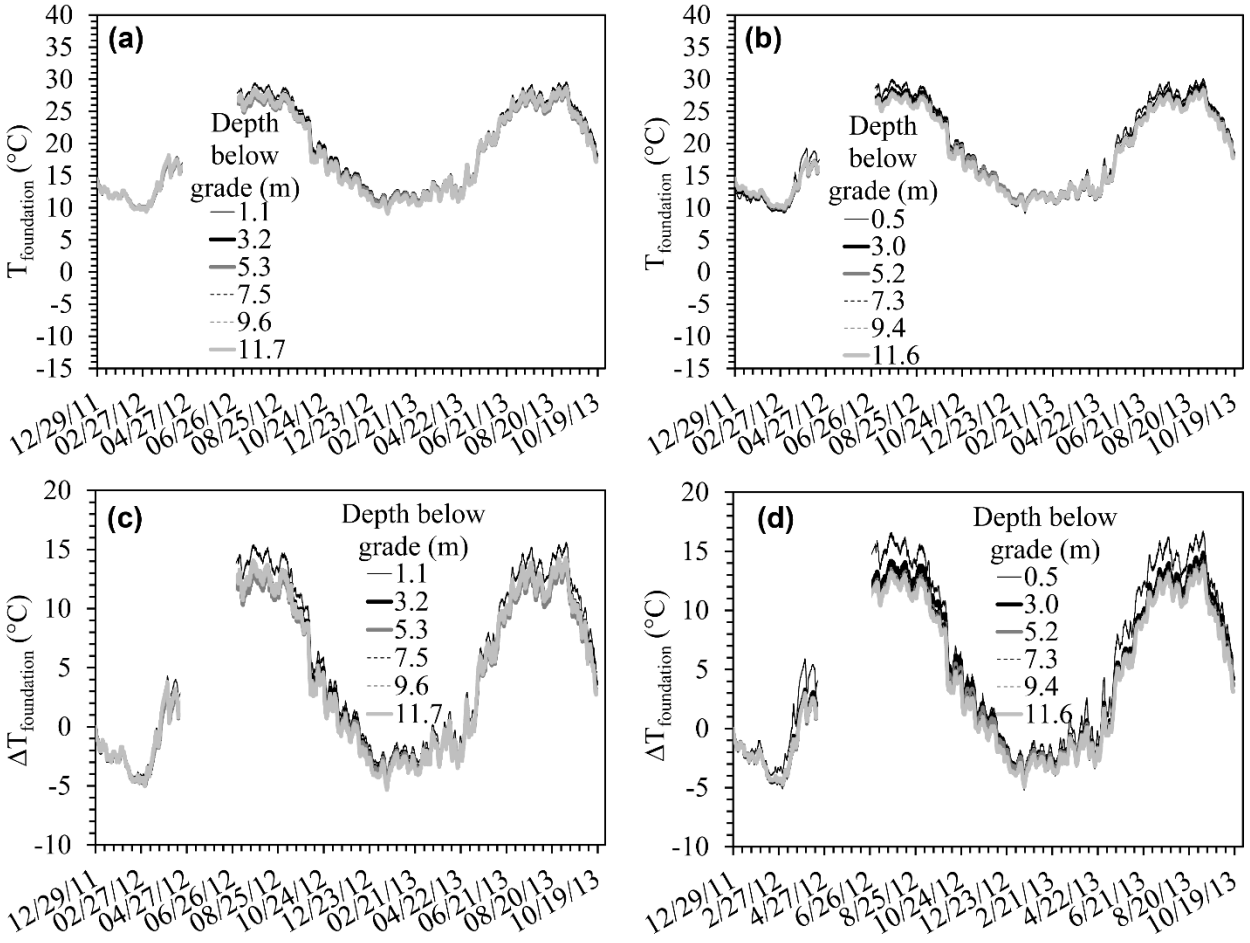

630

631 **FIG. 3.** Foundation temperatures: (a) Temperature fluctuations
632 in Foundation A; (b) Temperature fluctuations in Foundation B; (c)
633 Change in temperature in Foundation A; (d) Change of temperature in
634 Foundation B

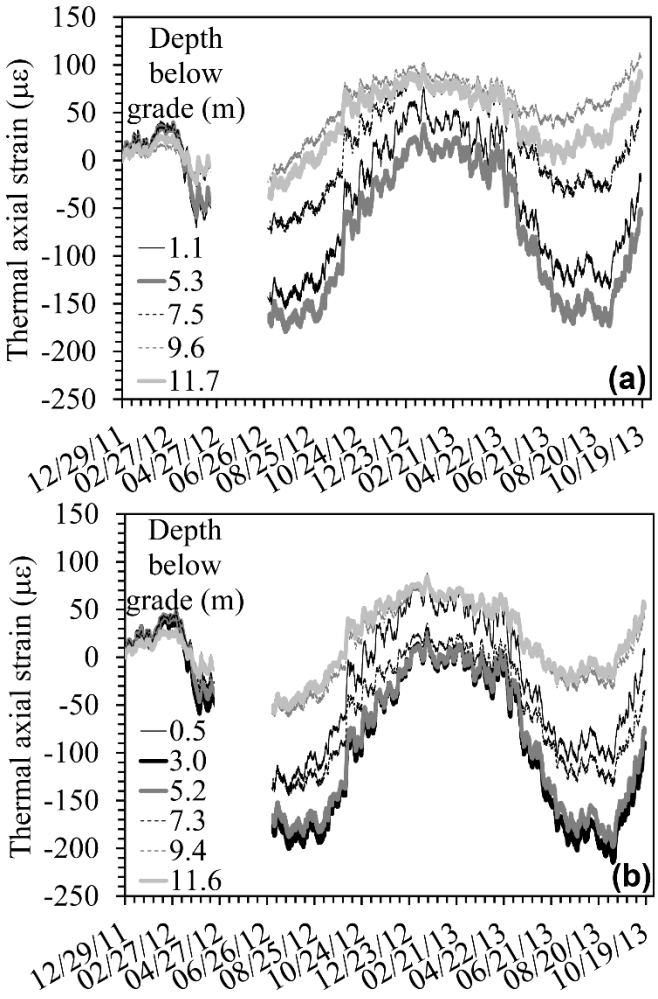

635

636 **FIG. 4.** Thermal axial strains: (a) Foundation A; (b) Foundation B

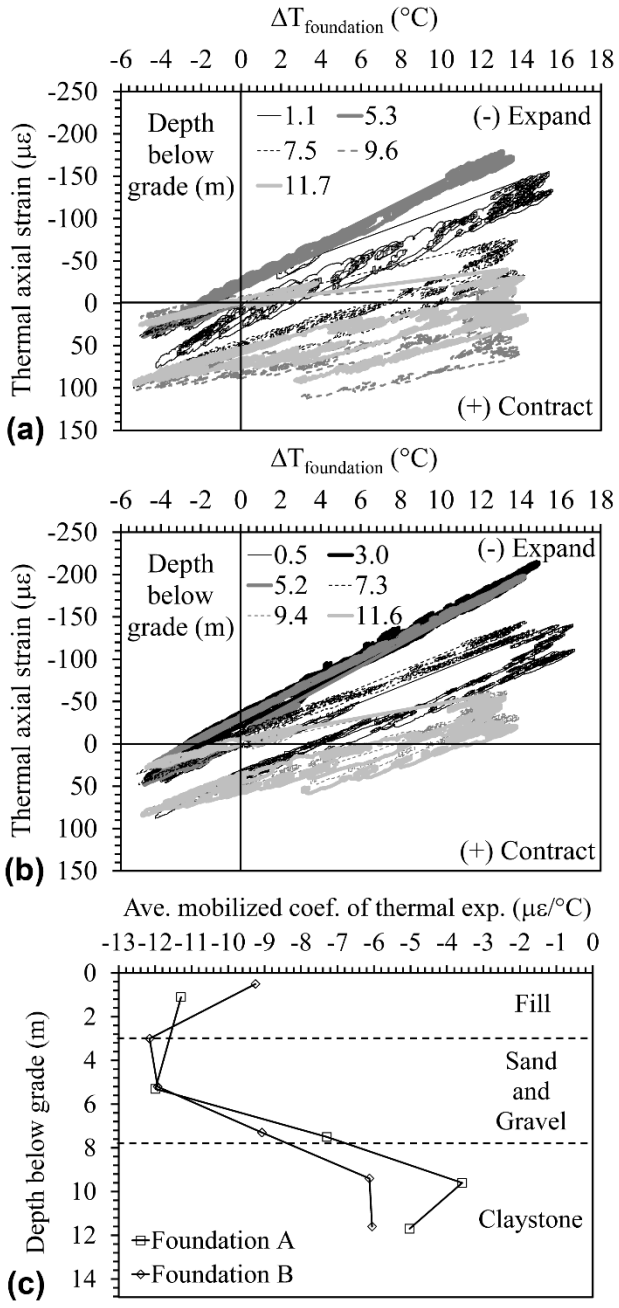

637

638 **FIG. 5.** Thermal expansion evaluation: (a) Thermal axial strain with change
639 in temperature for Foundation A; (b) Thermal axial strain with change
640 in temperature for Foundation B; (c) Distribution in average mobilized
641 coefficients of thermal expansion of the two energy foundations

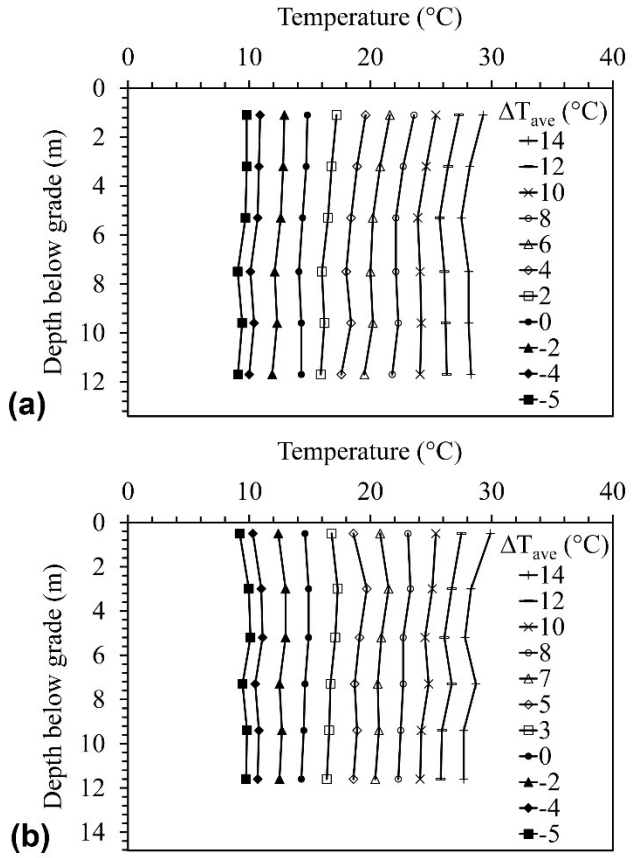

642

643 **FIG. 6.** Profiles of temperature for different average changes in foundation

644 temperature: (a) Foundation A; (b) Foundation B

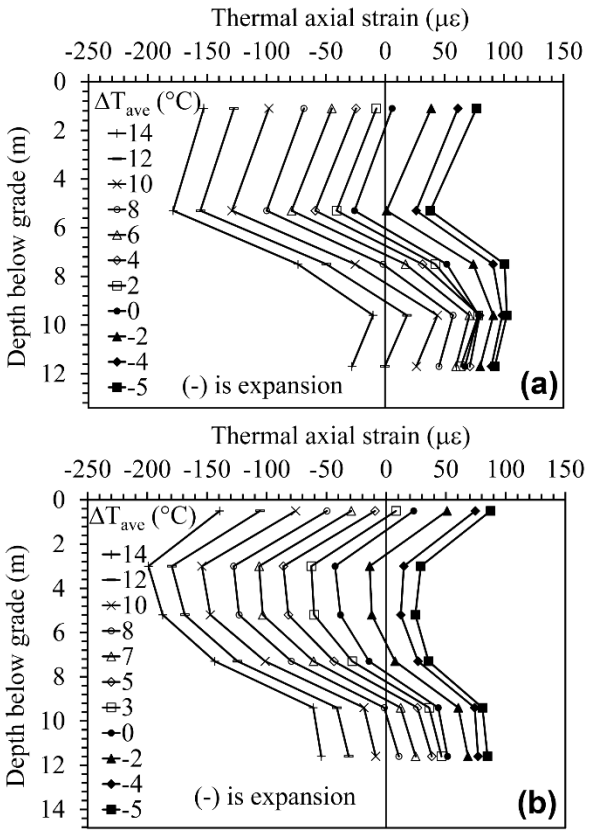

645

646 **FIG. 7.** Thermal axial strain profiles: (a) Foundation A: (b) Foundation B

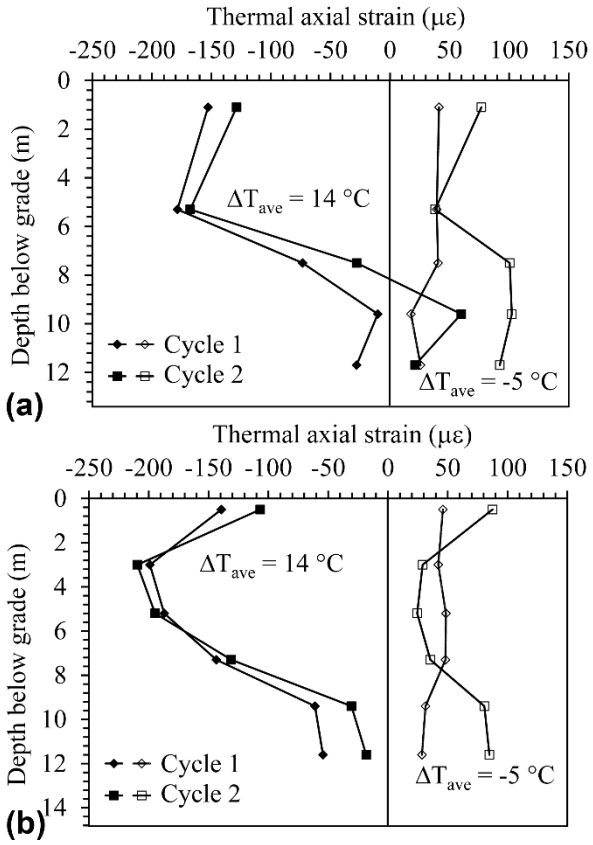

FIG. 8. Thermal axial strains after cycles of extreme temperature changes: (a) Foundation A; (b) Foundation B

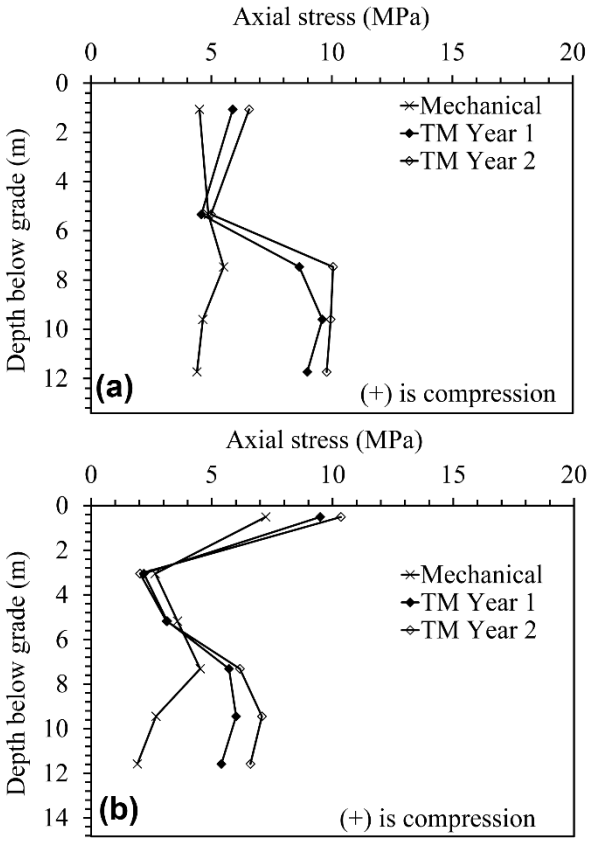

FIG. 9. Thermo-mechanical (TM) axial stresses during extreme heating to an average change in temperature of 14 °C: (a) Foundation A; (b) Foundation B

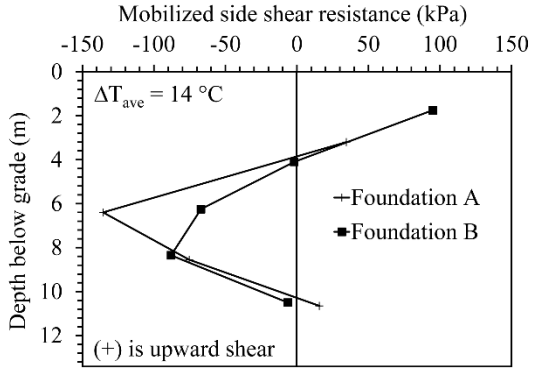

FIG. 10. Mobilized side shear resistance profiles during extreme heating to an average change in temperature of 14 °C for Foundations A and B

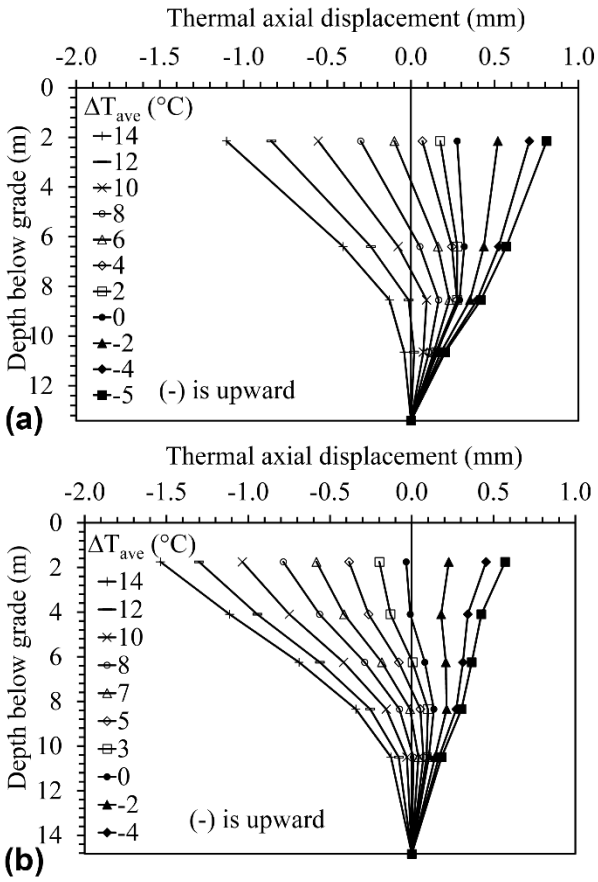

657

658 **FIG. 11.** Thermal axial displacements: (a) Foundation A; (b) Foundation B

659